Design and Analysis of A Mini Linear Optical Pickup Actuator

Joon Hyuk Park*, Yoon Su Baek, Young-Pil Park
Department of Mechanical Engineering, Yonsei University, 134, Shin-chon dong Sudae-mungu, Seoul 120-749, Korea

This paper describes a mini linear optical pickup actuator. To reduce the size, inner yokes are designed to guide the mover and outer yokes of permanent magnets are removed. Magnetic circuit method is used to determine the thrust force. Virtual path method is proposed to analyze the open magnetic circuit analysis. The magnetic circuit of the proposed actuator can be a closed circuit due to the virtual path model of the outer magnetic flux. The validity of virtual path method is evaluated by comparing to the FEM analysis. Structural vibration is investigated using FEM and the design of the mover is modified to improve the vibration characteristic. Dynamic characteristic experiments shows that the performance of the proposed actuator is enough to be used as a coarse and fine seeking actuator simultaneously and the thrust force margin for loading a focusing actuator is guaranteed.

Key Words: ODD (Optical Pickup Actuator), VCM (Voice Coil Motor), Virtual Path Method, Magnetic Circuit, Linear Actuator

1. Introduction

Optical disk drive is the one of the major information storage devices since it has the advantages of production cost, removability and portability. Main performance specification to improve those advantages can be classified into four parts, which are shorter access time, high transfer rate, high data capacity and smaller size.

Because the weight of an optical pickup is so large that the achievement of the high precision and high velocity motion of optical pickup is difficult with one stage type like swing arm of HDD, the conventional mechanism of the optical pickup for radial direction is composed of a coarse actuator and a fine actuator.

Therefore, to reduce the access time, performance of high force capability in the coarse actuator and high servo bandwidth in the fine actuator are required (Park et al., 2001). But optical pickup undergoes the transient vibration between coarse seeking mode and fine seeking mode and the waiting time is needed in order that the transient vibration may vanish. The waiting time is one of the important factors to disturb the fast access. Thus, research on the reduction of the waiting time is one of the major issues to enhance the performance the ODD (Park et al., 2002).

Recently, portable mini ODD is widely used and the requirement for small information storage device has been increased as the usage of personal digital assistants or other mobile computers are increased. If the ODD can be smal enough and have high data capacity, it will be very useful for mobile computers because of its unique advantages. But the general mechanism of optical pick up actuator for ODD has some difficulties to accomplish the small size because the dual stage type is used for radial direction actuator.

A linear actuator can be one of the suitable methods to overcome the weakness of the con-

* Corresponding Author,
E-mail : watchcon@yonsei.ac.kr
TEL : +82-2-2123-2827; **FAX** : +82-2-362-2736
Department of Mechanical Engineering, Yonsei University, 134, Shin-chon dong Sudae-mungu, Seoul 120-749, Korea. (Manuscript **Received** October 14, 2002; **Revised** August 12, 2003)

ventional mechanism of optical pickup actuator. It can eliminate the nonlinear factors like backlash of rack and pinion, make the weight reduction and have a larger force to weight ratio because it is a direct drive system. Its mechanical response is also faster (Basak and Filho, 1995; Choi et al., 1999). Therefore, it is suitable to make the ODD miniaturization. In addition, if the linear actuator can achieve the coarse and fine motion as a single servo, the waiting time until the transient vibration is vanished is not required.

In this paper, we suggest a VCM (voice coil motor) type mini linear actuator for optical disk drive and discuss the possibility of the application to the single servo type radial direction actuator. The mechanism design of a focusing actuator to be loaded on the proposed linear actuator will be discussed in the future study.

The proposed linear actuator should secure enough force constant to maintain the performance when the focusing actuator is loaded. Thus, thrust force should be modeled to estimate the force constant of the linear actuator. We use the magnetic circuit method to analyze the magnetic flux density that generates the thrust force with applied currents. To design magnetic circuit of the linear actuator, virtual path method is proposed.

The high servo bandwidth of the linear actuator should be guaranteed so that the proposed linear actuator can also fill the role of the fine actuator. To use the high servo bandwidth of the controller, force constant of the proposed actuator should be high and resonant frequency for the structural vibration of mover should be positioned at high region because the resonance of the structural vibration of mover is uncontrollable mode. Therefore, in this paper, FE analysis is used to estimate the vibration characteristic of the mover and improve the design.

The performance of the proposed linear actuator is estimated by dynamic characteristic experiments.

2. VCM Type Mini Linear Actuator

Figure 1 shows the proposed linear actuator. During the design of the proposed actuator, three design targets are considered : an enough thrust force, reducing the rotation moment and small size.

Firstly, to secure an enough thrust force, two coils and two permanent magnets are positioned at the both sides of the actuator. And yokes are located between the two permanent magnets to reduce the magnetic flux leakage. Magneto motive forces (MMFs) of two permanent magnets are connected in series to increase thrust force. Second, rotation moment can create the tilting of the mover since there exists the clearance between the guide and the mover, which is caused by manufacturing tolerance and/or assembly error. The tilting of the mover needs to be reduced because it decreases the system performance. To reduce the rotation moment due to the difference of the thrust force at both sides, this actuator is designed so that single magnetic flux passes through the air gaps and yokes. It also means that two permanent magnets are connected in series. Third, to reduce the size, inner yokes are designed to guide the mover and outer yokes of permanent magnets are removed. Therefore, the magnetic system of the proposed actuator is open circuit. Open circuit makes the efficiency of the magnetic flux decrease since flux leakage is larger than closed circuit. But decreased efficiency of the magnetic flux of the actuator can be compensated sufficiently because MMFs of the two permanent magnets are connected in series.

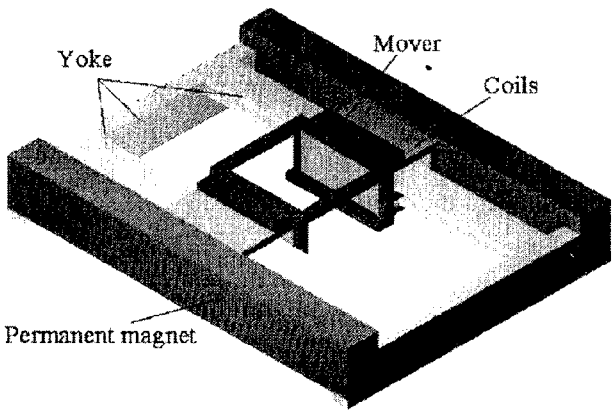

Fig. 1 The proposed mini linear actuator

3. Magnetic Analysis and Thrust Force Modeling

3.1 Virtual path model for magnetic circuit design

Magnetic circuit design including permanent magnets has been studied widely (Leupold, 1993 ; Tsai and Chang, 1999). But magnetic flux that passes through the outer air has usually been neglected by the difficulty of modeling. Therefore, we propose the virtual path method that can be used to model the outer magnetic flux by approximation. The magnetic circuit of the proposed actuator can be a closed circuit due to the virtual path model of the outer magnetic flux. Virtual path method can be useful for modeling of various kinds of open magnetic circuits if the virtual path shape is modified properly according to the condition.

The rudimentary concept of the virtual path method is that most of magnetic flux passes where the reluctance is minimum. Thus, proper shape of magnetic flux path for outer air is determined roughly and it is modified toward to minimizing the outer air reluctance.

To make the analysis simple, let us consider the magnetic circuit composed of only two right prim type permanent magnets as shown in Fig. 2. The each magnetic flux that passes between faces 1 and faces 2 is neglected because the property of the permanent magnets is considered as orthotropic.

Figure 2(a) shows the geometry of two permanent magnets. Faces A is divided into 16 sections. Each section of the face A has the virtual path independently. And all the virtual path directions are toward to the other face A because all the magnetic flux except one from the center of the permanent magnet should be curved theoretically.

To reduce the error, virtual path shape between the faces A should be selected properly. In this paper, small and half annulus and elliptical shape are used.

Magnetic flux is determined similar to the electric current as Eq. (1)

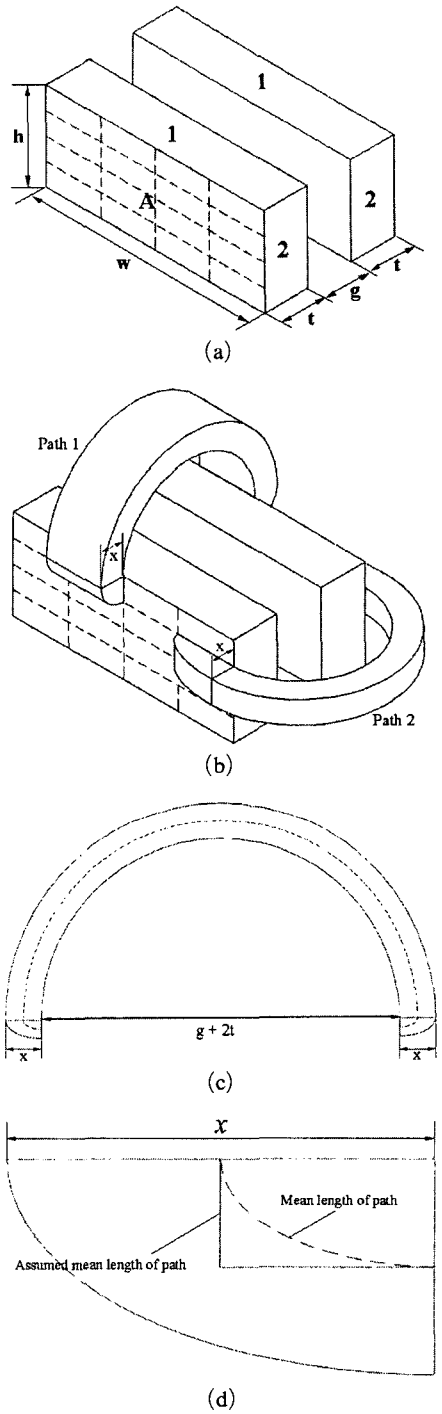

Fig. 2 Virtual path model for outer magnetic flux, (a) two identical right permanent magnet, (b) outer magnetic flux path model when, (c) flux path model by half annulus and quarter elliptical shapes and (d) elliptical shape part of flux path 1, 2

$$\phi=\frac{\Im_{PM}}{\Re} \tag{1}$$

where $\Im_{PM}$ is the magneto motive force and $\Re$ is the reluctance.

Because the magneto motive force can be calculated simply from the data sheet of the permanent magnet, magnetic flux can be obtained easily when the reluctance is determined. Therefore, the reluctance of virtual path model should be investigated first. Reluctance is determined as Eq. (2)

$$\Re=\frac{l}{\mu S} \tag{2}$$

where l is the mean length of magnetic flux path, S is the cross section area of the path and μ is the permeability.

Figure 2(b) shows the virtual path model. As shown in Fig. 2(c) and (d), virtual path is modeled using two elliptical shapes and a half annulus to consider the fringe path of magnetic flux. Reluctance of half annulus shape is well known (Roters, 1951). From Eq. (2), reluctance of the half annulus in the Path 1 can be expressed as

$$\Re_a=\frac{2\pi(g+2t+x)}{\mu_0 wx} \tag{3}$$

In the case of $g+2t<3x$,

$$\Re_a=\frac{4\pi}{\mu_0 w \ln\left(1+\frac{2x}{g+2t}\right)} \tag{4}$$

Similarly, reluctance of the half annulus in the Path 2 is,

$$\Re_a=\frac{2\pi(g+2t+x)}{\mu_0 hx} \tag{5}$$

In the case of $g+2t<3x$,

$$\Re_a=\frac{4\pi}{\mu_0 h \ln\left(1+\frac{2x}{(g+2t)}\right)} \tag{6}$$

Mean cross section area of the elliptical path should be used to find the reluctance of elliptical shape because the cross section area is different according to the path length. To make the problem simply, assuming that the mean length of the path is straight line as shown in Fig. 2(d), the mean length of the path is expressed as Eq. (7).

$$l=\frac{x}{2}+\frac{h}{8} \tag{7}$$

The mean cross section area can be estimated by dividing the entire volume of the path by the mean path length. Thus it is expressed as,

$$S=\frac{\pi xhw}{8}\cdot\frac{1}{\frac{x}{2}+\frac{h}{8}} \tag{8}$$

Substituting Eqs. (7) and (8) into Eq. (2), the reluctance of the elliptical shape in the Path 1 is determined as,

$$\Re_b=\frac{8\left(\frac{x}{2}+\frac{h}{8}\right)^2}{\mu_0\pi xhw} \tag{9}$$

Similarly, the reluctance of the elliptical shape in the Path 2 can be expressed as,

$$\Re_b=\frac{8\left(\frac{x}{2}+\frac{w}{8}\right)^2}{\mu_0\pi xwh} \tag{10}$$

Total reluctance of the Path 1 is the series connection of the reluctance of a half annulus and two elliptical shapes. Thus by the Eqs (3), (4) and (9), it is expressed as Eqs. (11) and (12).

$$\Re_1=\frac{2\pi(g+2t+x)}{\mu_0 wx}+\frac{16\left(\frac{x}{2}+\frac{h}{8}\right)^2}{\mu_0\pi xhw} \tag{11}$$

In the case of $g+2t<3x$,

$$\Re_1=\frac{4\pi}{\mu_0 w \ln\left(1+\frac{2x}{(g+2t)}\right)}+\frac{16\left(\frac{x}{2}+\frac{h}{8}\right)^2}{\mu_0\pi xhw} \tag{12}$$

Also, the total reluctance of the Path 2 is,

$$\Re_2=\frac{2\pi(g+2t+x)}{\mu_0 hx}+\frac{16\left(\frac{x}{2}+\frac{w}{8}\right)^2}{\mu_0\pi xwh} \tag{13}$$

In the case of $g+2t<3x$,

$$\Re_2=\frac{4\pi}{\mu_0 h \ln\left(1+\frac{2x}{(g+2t)}\right)}+\frac{16\left(\frac{x}{2}+\frac{w}{8}\right)^2}{\mu_0\pi xwh} \tag{14}$$

Entire virtual reluctance of the outer air is the parallel connection of eight pairs of virtual path reluctance. Thus it can be expressed as

$$\Re_t=\frac{k\cdot d}{32\pi\mu_0 hwx(k+d)} \tag{15}$$

where,

$$k=8\pi^2 gw+8\pi^2 w(x+2t)+(w+4x)^2$$
$$d=16x^2+h^2+8h(\pi^2 g+x+\pi^2(x+2t))$$

$$g+2t<3x$$
$$\Re_t=\frac{k\cdot d}{32\pi\mu_0 hwx\ln\left(1+\frac{2x}{g+2t}\right)(k+d)} \tag{16}$$

where,

$$k=16\pi^2 hx+(h+4x)^2\ln\left(1+\frac{2x}{g+2t}\right)$$
$$d=16\pi^2 wx+(w+4x)^2\ln\left(1+\frac{2x}{g+2t}\right)$$

Reluctance of the virtual path is the function of x because w, t, h and g are constants. According to the rudimentary concept of the virtual path model, x is determined to minimize the virtual reluctance, $\Re_t$ and minimum value of $\Re_t$ is the reluctance of the outer air. Thus, the entire reluctance of the outer air is as follows:

$$\Re_e=\mathrm{Min}\left[\frac{k\cdot d}{32\pi\mu_0 hwx(k+d)}\right] \tag{17}$$

In the case where $g+2t<3x$,

$$\Re_e=\mathrm{Min}\left[\frac{k\cdot d}{32\pi\mu_0 hwx(k+d)\ln(1+2x/(g+2t))}\right] \tag{18}$$

where $\mathrm{Min}[f(x)]$ is the minimum value of $f(x)$.

The validity of the virtual path method can be estimated from Fig. 3. There is a good agreement between the magnetic analysis by the magnetic circuit with virtual model and FEM. As the gap becomes smaller the error increases. This may be caused by the edge effect of the permanent magnets, which is neglected in the magnetic circuit analysis.

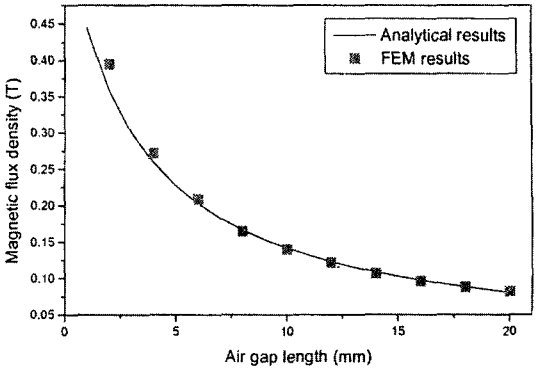

(a) 2 mm×22 mm×3 mm

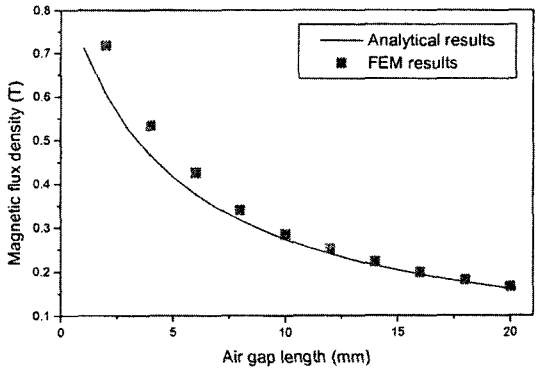

(b) 7 mm×10 mm×5 mm

Fig. 3 Magnetic flux density of air gap between two right prism type permanent magnets

3.2 Magnetic circuit design for proposed linear actuator

Figure 4 shows the magnetic circuit elements of the proposed linear actuator. $\Re_e$ indicates the reluctance of the outer air.

The reluctance of the air gap can be divided into two parts. One is the reluctance when magnetic flux flows toward to Yoke 2 and the other is when toward to Yoke 1 and 3. Figure 5 shows the magnetic flux path model of two parts.

Figure 5(a) shows the cross section of the center of yoke 2 and permanent magnet. Assuming that there is no magnet-end leakage that flows without the yoke, the reluctance of the air gap can be expressed as Eq. (19).

$$\Re_{a1}=\frac{\Re_f\Re_g}{\Re_f+\Re_g} \tag{19}$$

$\Re_{a2}$ is the same with $\Re_{a1}$ since the geometries are

the same. The magnetic flux path of the end side of permanent magnet must be modeled as Fig. 5 (b) with considering the effect of Yoke 1. It is determined as,

$$\Re_{end1}=\Re_{a1}+\Re_{Y1}+\Re_{o1} \tag{20}$$

All the reluctance of the both end sides of two permanent magnets can be calculated as Eq. (20) because the yokes of both end sides are symmetry and geometrically same. Thus magnetic reluctances of the air gaps and the end sides of the permanent magnets can be expressed as

$$\Re_{a1}=\Re_{a2}=\Re_a \tag{21}$$

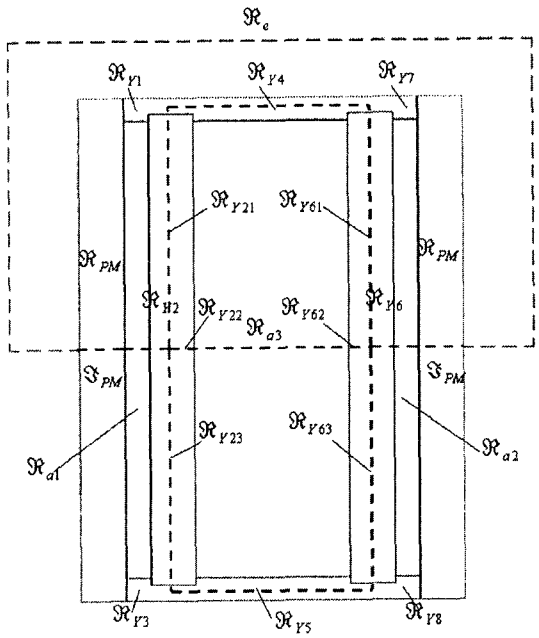

Fig. 4 Magnetic circuit elements of the total system

$$\Re_{end1}=\Re_{end2}=\Re_{end3}=\Re_{end4}=\Re_{END} \tag{22}$$

Based on the Figs. 4 and 5, the entire magnetic circuit of the proposed linear actuator can be designed as Fig. 6.

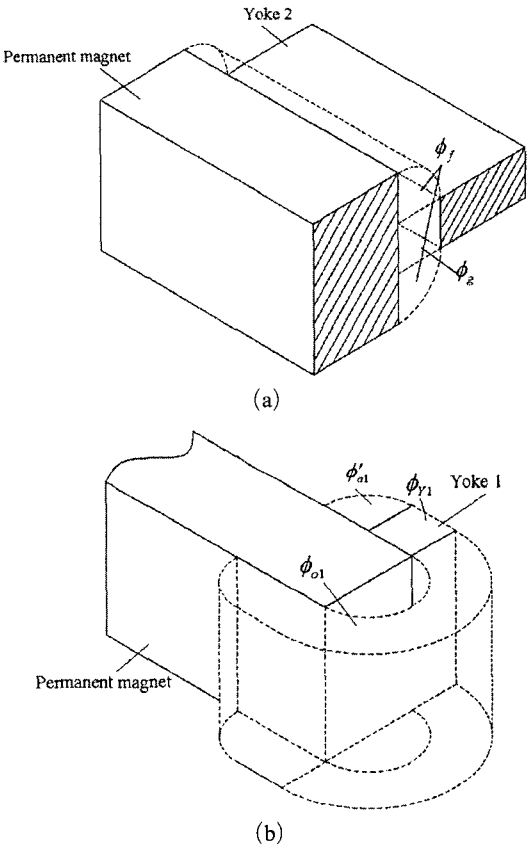

Fig. 5 Magnetic flux model for primary air gap of proposed linear motor, (a) at the center of the permanent magnet and primary yoke and (b) at the end of the permanent magnet

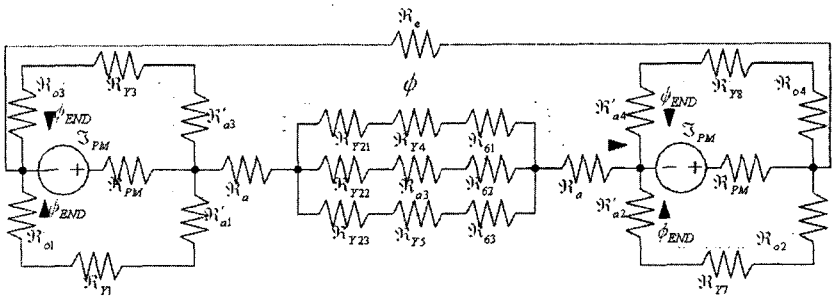

Fig. 6 Magnetic circuit diagram of the entire system

Where,

$\Im_{PM}$: Magneto motive force of the permanent magnet

$\Re_{Y1}$, $\Re_{Y3}$, $\Re_{Y5}$, $\Re_{Y7}$, $\Re_{Y8}$: Reluctances of the each yokes

$\Re_{Y21}$~$\Re_{Y23}$: Reluctance of the Yoke 2 according to the path where magnetic flux passes through

$\Re_{Y61}$~$\Re_{Y63}$: Reluctance of the Yoke 6 according to the path where magnetic flux passes through

$\Re_{PM}$: Reluctance of the permanent magnet

$\Re_{a1}$~$\Re_{a3}$: Reluctance of the each air gap

$\Re'_{a1}$, $\Re'_{a2}$: Reluctance of the air gap where the leakage of the magnetic flux flows

$\Re_{o1}$~$\Re_{o4}$: Reluctance of the air gap where the magnetic flux flows from Yoke 1, 3, 7, and 8, respectively

$\Re_e$: Reluctance of the outer air

Thus, the magnetic flux in the primary air gaps $\Re_{a1}(=\Re_{a2})$ can be calculated as

$$\begin{aligned}\phi=&2\Im_{PM}\Re_{END}(2\Re_a+\Re_{eq}+\Re_{END}+\Re_2)/\\&\{(2\Re_{eq}+4\Re_a+2\Re_e+\Re_{END})\\&\cdot(\Re_e\Re_{END}+2\Re_e\Re_{PM}+2\Re_{END}\Re_{PM}\\&+\Re_{eq}(\Re_{END}+2\Re_{PM})+2\Re_a(\Re_{END}+2\Re_{PM}))\}\end{aligned}\tag{23}$$

$\Re_{eq}$ is the equivalent reluctance composed by $\Re_{Y21}$~$\Re_{Y23}$, $\Re_{Y61}$~$\Re_{Y63}$, and $\Re_{a3}$ as Eq. (24).

$$\Re_{eq}=\frac{\Re_{eq1}\Re_{eq2}\Re_{eq3}}{\Re_{eq1}\Re_{eq2}+\Re_{eq2}\Re_{eq3}+\Re_{eq1}\Re_{eq3}}\tag{24}$$

where

$$\begin{aligned}\Re_{eq1}&=\Re_{Y21}+\Re_{Y4}+\Re_{Y61},\\\Re_{eq2}&=\Re_{Y22}+\Re_{Y3}+\Re_{Y62},\\\Re_{eq3}&=\Re_{Y23}+\Re_{Y5}+\Re_{Y63}\end{aligned}$$

The leakage of the magnetic flux at the end side of the permanent magnet is expressed as,

$$\begin{aligned}\phi_{END}=&4\Im_{PM}(\Re_{eq}+2\Re_a+\Re_e)(\Re_{eq}+2\Re_a+\Re_e+\Re_{END})/\\&\{(2\Re_{eq}+4\Re_a+2\Re_e+\Re_{END})\\&\cdot(\Re_e\Re_{END}+2\Re_e\Re_{PM}+2\Re_{END}\Re_{PM}\\&+\Re_{eq}(\Re_{END}+2\Re_{PM})+2\Re_a(\Re_{END}+2\Re_{PM}))\}\end{aligned}\tag{25}$$

Substituting Eqs. (19) into Eqs. (23), the magnetic flux and the leakage of the magnetic flux in the air gap can be expressed as Eqs. (26).

$$\begin{aligned}\phi=&2\Im_{PM}\Re_{END}\left(\frac{2\Re_f\Re_g}{\Re_f+\Re_g}+\Re_{eq}+\Re_{END}+\Re_e\right)\Big/\\&\left\{\left(2\Re_{eq}+\frac{4\Re_f\Re_g}{\Re_f+\Re_g}+2\Re_e+\Re_{END}\right)\right.\\&\cdot(\Re_e\Re_{END}+2\Re_e\Re_{PM}+2\Re_{END}\Re_{PM}+\Re_{eq}(\Re_{END}+2\Re_{PM})\\&\left.+\frac{2\Re_f\Re_g}{\Re_f+\Re_g}(\Re_{END}+2\Re_{PM})\right)\Big\}\end{aligned}\tag{26}$$

Using the magnetic circuit analysis with virtual path model, the magnetic flux density in the primary air gaps (B_g in Fig. 5(a)) is 0.310T and 0.253T in the fringe (B_f in Fig. 7(a)).

Figure 7 shows the magnetic flux density in the air gap by FEM. Magnetic flux density at the side of permanent magnet is larger than that of the center. It is due to the effect of yokes of both sides.

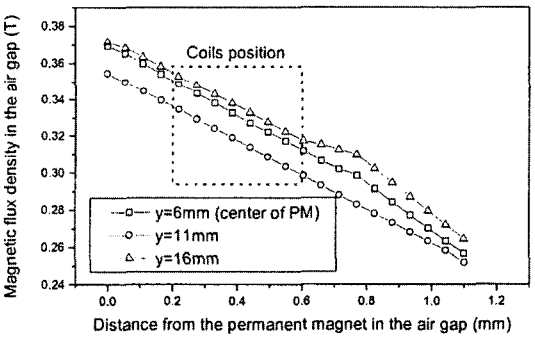

(a)

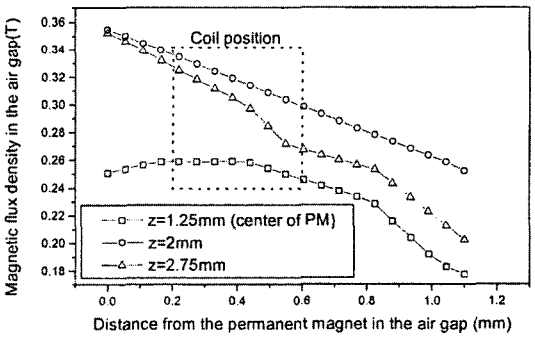

(b)

Fig. 7 Magnetic flux density in the air gap by FEM, (a) at the center, right and left parts of permanent magnet and (b) at the center, upper and lower parts of permanent magnet

But the magnetic flux densitx density at the center is larger than upper and lower parts of permenent magnet. Due to the yoke shape of the proposed linear actuator, there exists quite a little leakage of the magnetic flux at the lower part of the permanent magnet.

The average values of FEM results are 0.304T in the air gap and 0.281T in the fringe. The errors of the magnetic circuit analysis results are about 2% and 10% compared to FEM results, respectively.

3.3 Thrust force modeling

Thrust force of the proposed linear actuator is expressed from the Lorent's law (Popovič and Popovič, 2000),

$$\mathbf{F}=\int \mathbf{B}\times id\mathbf{l} \tag{27}$$

where, i is the currents of the coils, $\mathbf{B}$ is the magnetic flux density and $\mathbf{l}$ is the effective length of coils. Effective length of coils of the proposed actuator can be determined from Fig. 8.

The magnetic flux density that influences the coils is in the air gap and the fringe. Effective length of coils in the fringe region is different according to the number of layers. In the fringe, effective length of coil according to the layer can be expressed as Eq. (28).

$$l_f=\frac{l_{ff}-l_{fi}}{l_t/a-1}N+\frac{(l_t/a)\,l_{fi}-l_{ff}}{l_t/a-1},\quad N\geq 1 \tag{28}$$

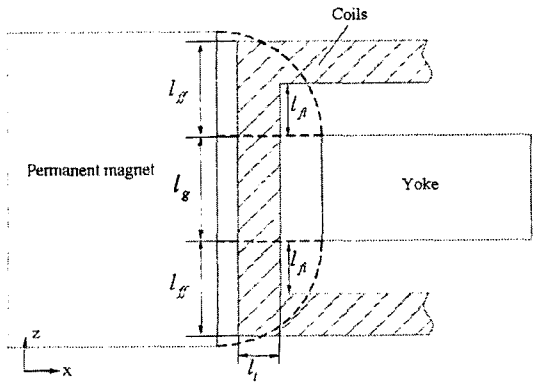

Fig. 8 Effective length of coil in the air gap and fringe path model

where, N is the number of layers and a is the diameter of the coil. Thus, from the Eqs. (27) and (28), the thrust force of the fringe can be determined as Eq. (29).

$$F_f=2\cdot iB_{fx}\cdot m\cdot\sum_{N=1}^{n}\left(\frac{l_{ff}-l_{fi}}{n-1}N+\frac{nl_{fi}-l_{ff}}{n-1}\right) \tag{29}$$

where, B_{fx} is the magnetic flux density of the fringe, m is the total number of turns of coil and n, that is determined as $n=l_t/a$, is the total number of layers of coils.

The effective length of coils in the air gap is $n\cdot l_g$ and thrust force of the air gap is determined as Eq. (30). Because two coils are located at both sides of the mover, entire thrust force can be expressed as Eq. (31).

$$F_g=iB_{gx}\cdot m\cdot n\cdot l_g \tag{30}$$

$$F=k_t\cdot i \tag{31}$$

where

$$k_t=\left(2\cdot B_{gx}\cdot m\cdot n\cdot l_g+4\cdot B_{fx}\cdot m\cdot\sum_{N=1}^{n}\left(\frac{l_{ff}-l_{fi}}{n-1}N+\frac{nl_{fi}-l_{ff}}{n-1}\right)\right).$$

Force constant k_t of the proposed actuator is shown on the Table 1.

Figure 9 shows the magnetic flux density in the working range of the mover. Magnetic flux density has the uniformity along the working direction. Therefore, force constant, k_t is independent of the working range and precision control is possible.

Table 1 Characteristic of mini linear actuator prototype

Size	Mover : 12.6×6×3.3 mm Total : 17×22×3.9 mm
Mass	Mover : 0.4 g
Permanent magnet	Material : NdFeB Remanence : 1.17 T
Coils	Resistance : 3.3 Ω Turns : 172×2 Inductance : 32 μH
Force constant	235 mN/A

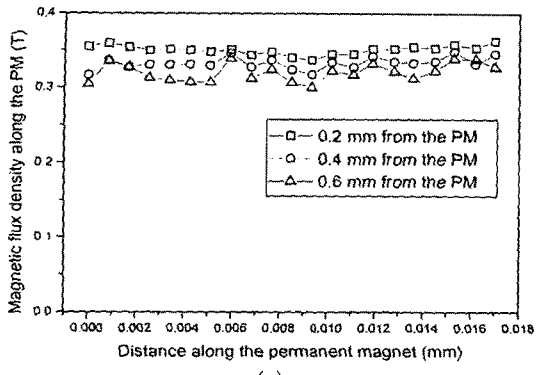

(a)

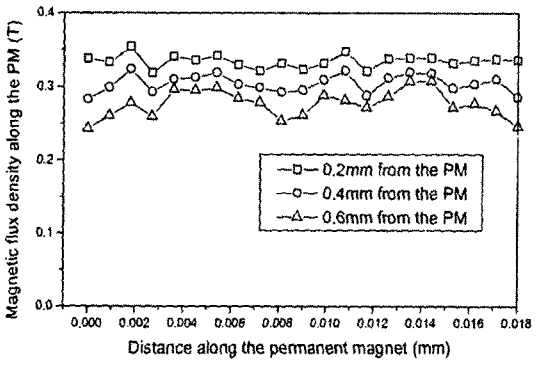

(b)

Fig. 9 Magnetic flux density of the air gap in the working range, (a) at the center of PM and (b) at the fringe part of PM

4. Vibration Characteristic of the Mover

Figure 10 shows the mover frame of the proposed linear actuator. Firstly, the flexible mode of the mover must be positioned over 300 Hz to be used as a coarse actuator. In this case, structural vibration resonant frequency over about 3kHz is allowed because uncontrollable mode should be positioned at ten times higher than servo bandwidth. To estimate the structural vibration characteristic of the proposed linear actuator, finite element method is used.

Figure 11(a) shows the first flexible mode of the mover frame. The first resonant frequency of the flexible mode is about 17.4 kHz. With coils, the first resonant frequency of the mover is about 3.7 kHz as shown in Fig. 11(b). It is because the coils have not influence on the stiffness but on

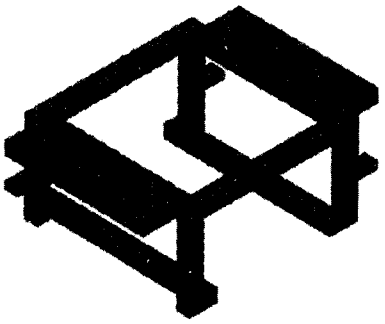

Fig. 10 The mover frame of the proposed liner actuator

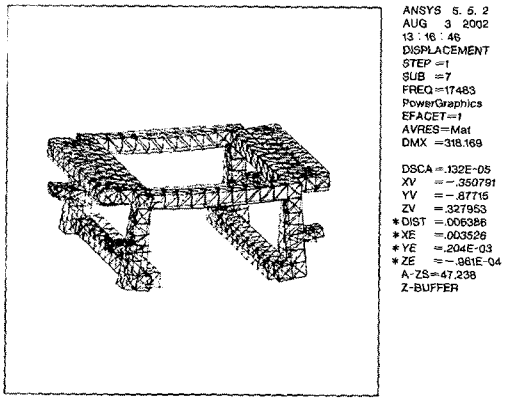

(a)

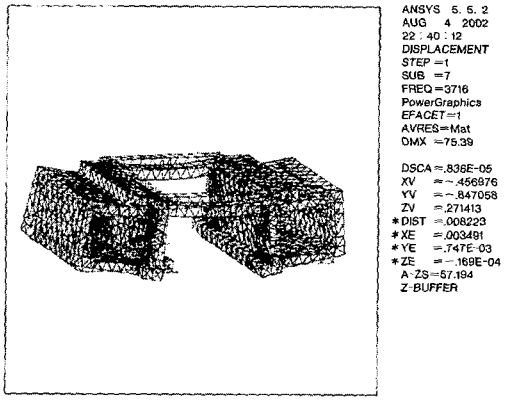

(b)

Fig. 11 First flexible mode of the mover, (a) mover frame and (b) with coils

the weight of the structure. But the servo bandwidth of the proposed linear actuator can be still 300 Hz.

In order to use the proposed linear actuator for the fine actuator as well as the coarse actuator, the

flexible mode of the mover should be positioned as high as possible and especially it has to be more than 20 kHz. Therefore, the structure of the mover must be modified to have the high servo bandwidth.

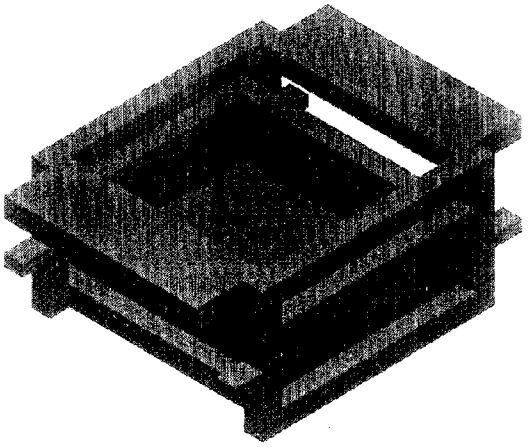

Fig. 12 Modified mover frame of the proposed linear actuator

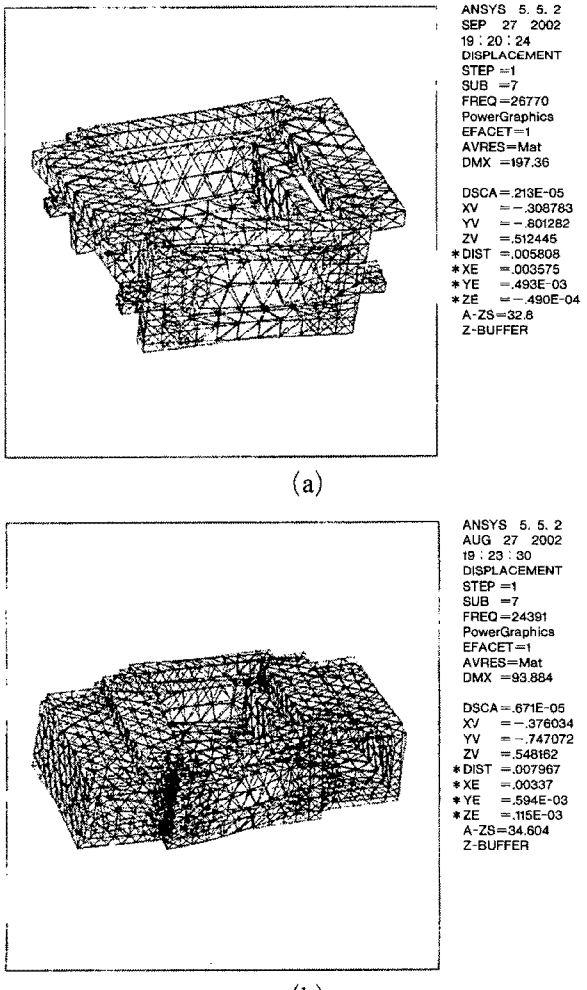

Fig. 13 First flexible mode of modified mover, (a) mover frame and (b) with coils

As shown in Fig. 11(b), the first mode shape is the bending mode and it can be predicted that the next will be shear mode from the structural shape. Thus, the mover is modified to prevent the first bending and shear mode.

Figure 12 shows the modified mover. To prevent the bending mode, bottom plate of the mover is attached and four plates are attached to each side faces to prevent shear mode. The reinforcement material is the same as mover's and the size is decided from the trial and error with FE analysis. Figure 13(a) shows the flexible mode of the modified mover frame and Fig. 13(b) shows the flexible mode of the modified mover with coils. The resonant frequencies are 26.8 and 24.4 kHz, respectively. Therefore, the proposed linear actuator can be used for the coarse and fine actuator and the servo bandwidth can be expanded into 2.4 kHz.

5. Experiments

Figure 14 shows the prototype of the proposed linear actuator. The characteristic of prototype is described in the Table 1. Two coils are parallel connected. It has more advantage than the series connection from the viewpoint of power efficiency if the resistances of coils are the same.

The performance of the mini linear actuator can be estimated from the dynamic characteristic. Assuming that nonlinear factors like friction and stiffness of wire can be neglected, transfer function for displacement of the actuator can be expressed as

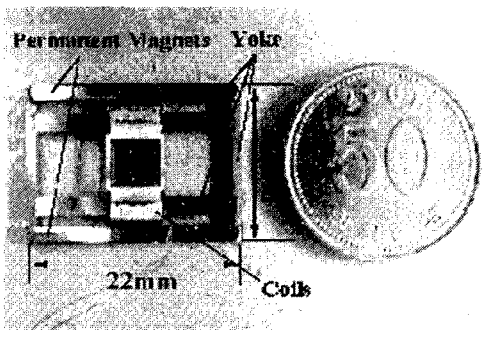

Fig. 14 Prototype of the mini linear actuator

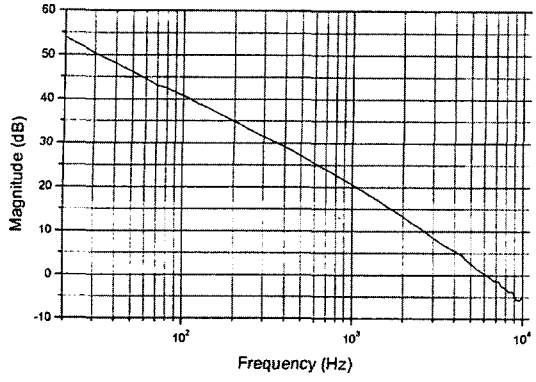

(a)

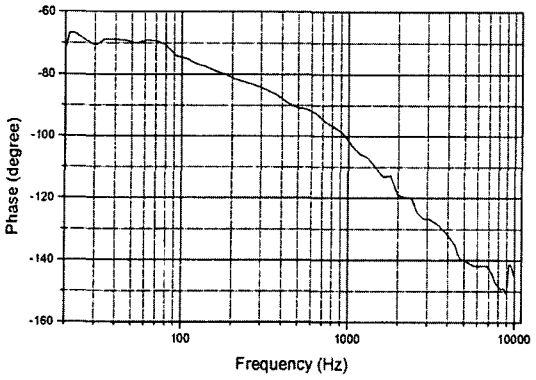

(b)

Fig. 15 Frequency response of the velocity of the prototype actuator

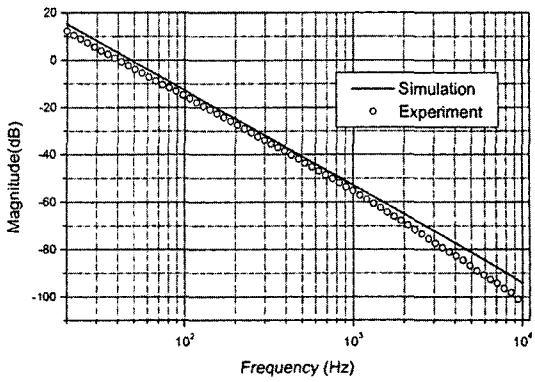

(a)

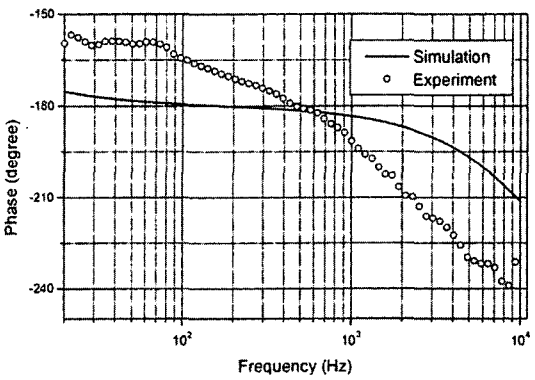

(b)

Fig. 16 Frequency response of the displacement the prototype actuator

$$\frac{H(s)}{V(s)}=\frac{k_t}{mLs^3+Rms^2+k_t^2 s} \tag{32}$$

where L and R is the inductance and electric resistance of the coils respectively, m is the mass of the mover and k_t is the force constant.

Figure 15 shows the experiment results for the frequency response of the velocity of the actuator and Fig. 16 shows the frequency response of the displacement of the actuator when the amplitude of the input voltage is 1 V. The magnitudes in Figs. 15 and 16 are the ratios of outputs to unit inputs, 1 mm/s and 1 mm, respectively. The magnitudes of the velocity and displacement of the actuator are 501 mm/s and 4 mm, respectively when the frequency of the input voltage is 20 Hz.

Because of the nonlinear factors that are neglected in the Eq. (32), there are a little bit differences between experiment results and simulation. Especially, experimental results shows that the phase drop below −80 degree appears more faster than simulation. Controller can compensate these nonlinear effects but they deal somewhat additional loads to the controller. Thus, estimation and improvement of nonlinear effects is needed. But from the experiment and simulation results, we can conclude that force constant, that is D.C gain of the proposed actuator, is large enough to generate the desired acceleration and thrust force margin for loading a focusing actuator is guaranteed.

6. Conclusion

In this paper, we suggest a VCM type mini linear actuator for optical disk dive. This actuator is designed that inner yokes can guide the mover and outer yokes of permanent magnets is removed. To reduce the moment of rotation, it is

designed so that single magnetic flux generates the thrust force.

Virtual path method is proposed to analyze outer magnetic flux. Using the magnetic circuit method with virtual path model, magnetic flux density of the air gaps and thrust force were modeled. The validity of the virtual path method is estimated by comparing to FEM. Virtual path model is applicable to analyze the open magnetic circuit including permanent magnets.

To use the mini linear actuator for the fine actuator as well as coarse actuator simultaneously, the structure of the mover was modified. As a result, first flexible mode of the mover appeared at 24.4 kHz.

Frequency response of the actuator was experimented to estimate the performance. As a result, the difference of the phase between the simulation and experiment appeared intensely because of nonlinear effects. To reduce the nonlinear effect, research for reducing friction is needed since friction is more dominant than any other factors when inertia of the mover is so small in sliding system.

Experiment results show that the proposed linear actuator can be used as a radial direction actuator and has the thrust force margin enough to load the focusing actuator later.

From the experiment and structural vibration analysis by FEM, the validity of the proposed actuator for the coarse and fine actuator is verified.

In future studies, identification and improvement for friction force will be carried out. And we will improve the design to enhance the performance. Focusing actuator for mini VCM type linear actuator will be developed and the availability of the entire systems will be investigated as an optical pick up actuator.

Acknowledgment

This work was supported by the Korea Science and Engineering Foundation (KOSEF) through the CISD at Yonsei University under Grant No. R11-1997-042-09000l-0.

References

Basak, A. and Filho, A. F., 1995, "Investigation of a Novel Double Armature Brushless D.C. Linear Motor," *IEEE Industry Applications Conference*, Vol. 1, pp. 789~795.

Choi, C., Tsao, T.-C. and Matsubara, A., 1999, "Control of Linear Motor Machine Tool Feed Drives for End Milling: Robust MIMO Approach," *Proceedings of the American Control Conference*, pp. 3723~3727.

Leupold, H. A., 1993, "Approaches to Permanent Magnet Circuit Design," *IEEE Transactions on Magnetics*, Vol. 29, No. 6, pp. 2341~2346.

Park, J. H., Lee, S. H. and Baek, Y. S., 2002, "Mechanism Design of Optical Pickup Actuator for Fast Access of Optical Disk Drive," *KSPE*, Vol. 19, No. 12, pp. 109~119.

Park, K. H., Choi, C. H. and Ryu, J., 2001, "Hybrid Actuator for High Speed and High Precision Optical Disk Drives," Mechatronics, 11, pp. 527~543.

Popović, Z. and Popović, B. D., 2000, Introductory Electromagnetics, Prentice Hall, Inc.

Roters, H. C., 1951, Electromagnetic Devices, John Wiley & Sons, Inc., 1st edition.

Tsai, W.-B. and Chang, T.-Y., 1999, "Analysis of Flux Leakage in a Brushless Permanent-Magnet Motor with Embedded Magnets," *IEEE Transactions on Magnetics*, Vol. 35, No. 1.